The effect of bubbles on the wall drag in a turbulent channel flow

Jiacai Lu, Arturo Fernández, and Gretar Tryggvason[a)]
Worcester Polytechnic Institute, Worcester, Massachusetts 01609

(Received 14 September 2004; accepted 14 June 2005; published online 30 August 2005)

The effect of a few relatively large bubbles injected near the walls on the wall drag in the "minimum turbulent channel" is examined by direct numerical simulations. A front-tracking/finite-volume method is used to fully resolve all flow scales including the bubbles and the flow around them. The Reynolds number, using the friction velocity and the channel half-height, is 135 and the bubbles are 54 wall units in diameter. The results show that deformable bubbles can lead to significant reduction of the wall drag by suppression of streamwise vorticity. Less deformable bubbles, on the other hand, are slowed down by the viscous sublayer and lead to a large increase in drag. © *2005 American Institute of Physics*. [DOI: 10.1063/1.2033547]

INTRODUCTION

Experimental studies have demonstrated that the injection of air into a turbulent boundary layer can lead to significant reduction of the wall drag. The earliest study appears to be that of McCormick and Bhattacharyya[1] who found that microbubbles generated by electrolysis reduced the drag of a submerged body. Subsequent investigations by Madavan *et al.*,[2,3] using a flat plate mounted horizontally, with bubbles injected below it, found drag reduction of up to 80%. See also Ref. 4 for a review. While the early studies were motivated by applications to high-speed naval vessels or projectiles, later work by Japanese researchers has focused on commercial vessels, where viscous drag accounts for most of the total drag. For an overview of this work see Ref. 5. Even a relatively small reduction of the total drag can result in substantial fuel savings for both commercial and naval ships and/or shortened transit time. While drag reduction using relatively small amount of air, forming bubbles, has been demonstrated experimentally, obtaining detailed information about the exact mechanism has been nearly impossible due the difficulty of measuring the velocity field and the bubble distribution. Although theoretical models based on mixing length theories have been proposed (see Ref. 6, for example), they have not been based on detailed data.

It is well known that bubbles can have significant effect on vortical flows. In the simplest case, the bubbles simply reduce the average density of the liquid and can lead to baroclinic vorticity generation on a scale much larger than the bubble size. This is, for example, the case when a bubble cloud rises in an otherwise quiescent liquid. Bubbles can modify turbulent flows, as discussed by Lance and Bataille,[7] and Sridhar and Katz[8] have shown that even a few bubbles entrained into a large vortex can affect the vortical structure in a very significant way. It is also known that it is possible to manipulate turbulent boundary layers in various ways to reduce the wall drag. Du and Karniadakis[9] found, for example, that transverse-traveling waves could generate up to 50% drag reduction and several researchers (see Ref. 10 for a recent contribution) have shown that the addition of polymers into a turbulent boundary layer can reduce drag significantly. Thus, it is likely that the reason for drag reduction when bubbles are injected into a turbulent boundary layer can be found by examining the changes in the vortical structures of the flow.

In the absence of an understanding of the exact mechanisms, design and optimization of injection systems is difficult. Direct numerical simulations (DNS), where the flow field is found by solving the governing equations numerically on sufficiently fine grids so that all details, including the flow around the bubbles and their shapes, are fully resolved, should be able to yield the necessary insight. While DNS of homogeneous flows have a long history, DNS of multiphase flows, where it is necessary to account for the moving and deforming phase boundary, are more recent. Numerical simulations including the interactions between the bubbles and the fluid using simplified models have predicted drag reduction[11,12] but DNS accounting for the full interactions have so far not showed any significant change in the wall friction drag.[13,14] Here, we present DNS of the effects of bubbles on a turbulent flow, using relatively few bubbles in a small channel with a constant flow rate, that show significant drag reduction when the bubbles are deformable. While the Reynolds number and the domain are small, we believe that the results may apply to more general situations and we use the detailed data produced by the simulations to propose a mechanism for how the drag reduction takes place.

Our intention is to study the effect of relatively large bubbles, such as those generated by the injection of air through a porous plate in the wall where the bubbles form by a breakup of the air stream. This process generally results in bubbles of the order of 100 wall units or so. See Ref. 15 for recent experiments of this situation. The focus in this paper is therefore very different than in Ref. 12, where the effect of a large number of bubbles with a diameter of 2.4 wall units in a turbulent boundary layer was studied numerically using fully resolved flow and a point particle model for the bubbles. Such modeling, although clearly inappropriate for

[a)]Author to whom correspondence should be addressed. Telephone: (508) 831-5759. Fax: (508) 831-5680. Electronic mail: gretar@wpi.edu

the larger bubbles examined here, may yield accurate results for such small bubbles.

PROBLEM SPECIFICATION AND NUMERICAL METHOD

To keep the computer time required for each simulation to manageable levels, we have elected to examine the flow in the so-called "minimum turbulent channel." Jimenez and Moin[16] showed that while turbulent flow could be sustained in this channel, reducing it further damped out the turbulence. The domain size is $\pi \times \pi/2 \times 2$ units in the streamwise, spanwise, and wall-normal directions, respectively, with periodic boundaries in the streamwise and spanwise directions and rigid walls in the third direction. The flow rate is kept constant with an average velocity $U=0.6667$ by dynamically adjusting the pressure gradient. The fluid density is $\rho=1$ and the fluid kinematic viscosity is $\nu=1/3000$. The channel Reynolds number, $\mathrm{Re}_{H/2}=UH/\nu$, where $H=2$ is the height of the channel, is therefore 4000. For the flow without bubbles the average pressure gradient needed to keep the flow rate constant is 0.002 025. In terms of wall units, defined by $l_o^+=\nu/u^+$ where $u^+=\sqrt{\tau_w/\rho}$ is the friction velocity and τ_w is the average wall shear without bubbles, the size of the channel is $424\times 212\times 270$ and the Reynolds number using the friction velocity and the half-height of the channel is $\mathrm{Re}^+=u^+H/2\nu=135$. The diameter of the nondeformed bubble is $d_0=0.4$ or 54 wall units and surface tension ranges from 0.002 to 0.004. We have examined three different Weber numbers, $\mathrm{We}=\rho d_0(u^*)^2/\sigma$, equal to 0.203, 0.270, and 0.405. The bubbles can therefore deform, particularly in regions of high shear. Note that the Weber number defined in terms of the friction velocity is equal to a Capillary number $(\mathrm{Ca}=\mu V/\sigma)$ if the velocity V is taken to be the velocity difference across the bubble, given by $V=d_0(du/dy) =d_0(\tau_w/\mu)$. The size of the bubbles (in wall units) was selected to be comparable to those found in experimental studies where air is injected through a hole or a porous plate in the wall, and the bubbles form by a breakup of the air stream.[15] To make the simulations as easy as possible, the density of the bubbles is one-tenth of the liquid density. The viscosity of the bubbles and of the liquid are taken to be equal, so the kinetic viscosity of the bubbles is ten times that of water, comparable to what it is for air and water. This high viscosity reduces the mobility of the bubble surface but has little effect on the deformability of the bubbles. Small air bubbles in water usually have a nearly immobile surface due to contaminants and while the effect is not exactly the same as increasing the viscosity, it is considerably easier to implement numerically. For the simulations reported here, we follow the motion of 16 bubbles, with eight bubbles initially located near each wall in a slightly perturbed regular array at a distance of 0.375, or 50.6 wall units, from the wall. The time for a fluid particle moving with the average velocity to go through the channel once is 4.71 in computational units and by the time the simulations are stopped (time 55 in computational units) the bubbles have moved about 11.7 times through the domain. When we present the results, we nondimensionalize time by dividing by $t^+=\mu/\tau_w$. Other nondimensionalizations are explained in the figure captions.

To fully resolve the fluid flow around each bubble and to account accurately for bubble-bubble interactions and bubble deformation, the computations were carried out by a finite-volume/front-tracking technique where one set of equations is used for the whole domain, including both the bubbles and the carrying liquid. The "one-fluid" Navier-Stokes equations is as follows:[17,18]

$$\rho\frac{\partial \mathbf{u}}{\partial t}+\rho\nabla\cdot\mathbf{u}\mathbf{u}=-\nabla P+\nabla\cdot\mu(\nabla\mathbf{u}+\nabla\mathbf{u}^T)+\sigma\int_F \kappa_f\mathbf{n}_f\delta(\mathbf{x}-\mathbf{x}_f)dA_f. \tag{1}$$

Here, $\mathbf{u}$ is the velocity, P is the pressure, and ρ and μ are the discontinuous density and viscosity fields, respectively. δ is a three-dimensional δ function constructed by repeated multiplication of one-dimensional δ functions. κ is twice the mean curvature. $\mathbf{n}$ is a unit vector normal to the front. Formally, the integral is over the entire front, thereby adding the δ functions together to create a force that is concentrated at the interface but smooth along the front. $\mathbf{x}$ is the point at which the equation is evaluated and $\mathbf{x}_f$ is the position of the front. The singular term ensures that the momentum equation implicitly contains the correct stress boundary conditions at the interface. Both the liquid and the air are taken to be incompressible, so the mass conservation equation reduces to

$$\nabla\cdot\mathbf{u}=0 \tag{2}$$

for the whole flow field. We also take the density and viscosity of each fluid to be constants.

The Navier-Stokes equations are solved by a second-order accurate projection method, using centered differences on a fixed, staggered grid. The bubble surface (the "front") is explicitly marked by connected marker points that form an unstructured triangular grid. The front points are advected by the flow velocity, interpolated from the fixed grid. The front is used to update the density and viscosity at each grid point and to find the surface tension. As the front deforms, surface markers are dynamically added and deleted. The surface tension is represented by a distribution of singularities (δ functions) located at the front. The gradients of the density and viscosity become δ functions when the change is abrupt across the boundary. To transfer the front singularities to the fixed grid, the δ functions are approximated by smoother functions with a compact support on the fixed grid. At each time step, after the front has been advected, the density and the viscosity fields are reconstructed by integration of the smooth grid δ function. The surface tension is then added to the nodal values of the discrete Navier-Stokes equations. Finally, an elliptic pressure equation is solved by a multigrid method to impose a divergence-free velocity field. For a detailed description of the original method, including various validation studies, see Refs. 17 and 18. We note that the only other simulations of fully deformable bubbles in turbulent flows, by Kanai and Miyata,[13] and Kawamura and Kodama,[14] have been done using a similar approach.

For the simulations presented here we started with a fully parallel code written in FORTRAN 90/95 for the simulations described by Bunner and Tryggvason.[19] Three major changes were, however, necessary for simulations of bubbles in a turbulent channel flow. First of all, as the Reynolds number is increased, the resolution requirement increases, particularly at the wall. We have therefore changed the code to accommodate nonuniform grids in the direction normal to the wall. The grid spacing in the streamwise and the spanwise direction is uniform. Secondly, the demand on the advection solver also increases as the Reynolds number increases and we have implemented a third-order upwind scheme (QUICK) to allow us to accurately deal with such systems.[20] Higher-order upwind schemes generally require a broader stencil than the centered difference scheme used earlier in the code and implementing the new scheme therefore affects the parallelization as well. And thirdly, for high Reynolds numbers we found increasing irregularities in the velocities near the front with the original code. The original code used a conservative form of the governing equations and we found that a slight inconsistency between the advection of density and momentum was eliminated by using the nonconservative form of the advection terms. Rudman[21] reported a similar problem and the same remedy for a Volume of Fluid (VOF) method. The new code was tested extensively by comparing it with the original code (which has been thoroughly validated) and by grid refinement studies.

The computations were done using grids with $256 \times 128 \times 256$ grid points, uniformly spaced in the streamwise and the spanwise direction but unevenly spaced in the wall-normal direction. The smallest cell, near the wall, was 0.2104 wall units thick and the largest cell, at the center of the channel, was 1.670 units thick. To avoid having to compute the transition of the flow to turbulence, an already existing dataset was used for the initial turbulent flow,[22] and the bubbles inserted near the walls at time zero. The initial data were computed using $65 \times 65 \times 65$ modes, and were interpolated to generate initial data on the finer grid used in our simulations. Before adding the bubbles, we continued the turbulence simulation to confirm that our code preserves the statistics of the flow. Several years ago there was some debate about the use of second-order finite difference methods for turbulence simulations but our tests, in agreement with other recent work such as that of Orlandi,[23] confirmed that such methods indeed give results comparable to those produced by higher-order spectral codes.

RESULTS

In Fig. 1 the bubbles and isocontours of the streamwise vorticity are shown at two times, for turbulent flow without bubbles (top row) and for two simulations with bubbles. In the middle row We=0.203 and the bubbles deform relatively little except those very close to the wall, but in the bottom row, where We=0.405, the bubbles can deform more. The left column shows the flow at $t=24.3$, shortly after the bubbles are inserted into the flow. At this time the bubble distribution is essentially the same for both cases and many aspects of the vortical structures are the same for the bubbly flows as for the flow without bubbles. The right column shows the flow at $t=267.3$, after the bubbles have had time to modify the turbulence. Here there is significant difference both in the positions of the bubbles and the vortical structures between the different cases. The yellow isocontour surfaces denote positive vorticity and the blue green indicates negative vorticities. As is typical of wall-bounded turbulent flows, the vortices are predominantly near the wall, aligned in the streamwise direction. Although not very clear in the figure, the positive and negative vorticity generally alternate and for vortices close to the walls, there are wall-bounded vortices of the opposite sign to satisfy the no-slip boundary conditions. It is clear that for the We=0.405 case the presence of the bubbles has resulted in significant suppression of the streamwise vorticity and a careful study of the figure (as well as other figures that are not included) shows that next to the walls the bubbles squeeze the vortices toward the wall as they move over them. In addition to the bubbles and the vorticity, the shear stress on the bottom wall is also shown using color contours. Blue is low shear stress and red is high. As expected for turbulent flows, the regions of high and low shear appear as streaks elongated in the flow direction. While the view of the bottom is partially obscured by the presence of the bubbles and the vortices, it should be clear that at a late time there is a significant reduction in regions of high shear for the most deformable bubbles.

Figure 2 shows a close-up of one of the bubbles near the top wall, from the simulations in Fig. 1 at time 24.3, looking down the channel. In the frame on the right the bubbles deform significantly (We=0.405) and in the left frame the bubbles remain nearly spherical (We=0.203), except those very close to the wall. The velocity in a plane through the middle of the bubble is shown by arrows and the streamwise velocity in that plane is shown by color contours. The velocity is plotted at every grid point, giving an indication of the resolution used for the simulations. There is a significant difference to the degree that the bubbles are deformed, and while the low We bubble is not completely spherical, its deformation is relatively small compared to the high We bubble. The deformable bubble is stretched in the flow direction (the top part of the bubble is behind the plane in which the velocity is shown) as well as tilted toward the left. At this early time the bubble has not affected the flow significantly, although some differences are seen, particularly on the right where the streamwise vortex is closer to the wall for the deformed bubble.

The mean wall shear on the top and the bottom wall is plotted versus time in Fig. 3 for the flow without bubbles and the three simulations with bubbles. The flow rate is constant, and since the domain is fairly small and the flow structure changes with time, the total wall drag also changes with time, even in the absence of bubbles. For the flow without bubbles, however, the time-averaged value should remain constant if we ran the simulation for a long enough time. The evolution of the wall drag depends strongly on the deformability of the bubbles, although the initial adjustment, after the bubbles are added at time zero, is similar for all three cases. For the most deformable bubbles (We=0.405) the drag gradually decreases and by time 300 the total drag on both walls has been reduced by nearly 20%. Although the drag on the bottom wall continues to decrease, the drag on

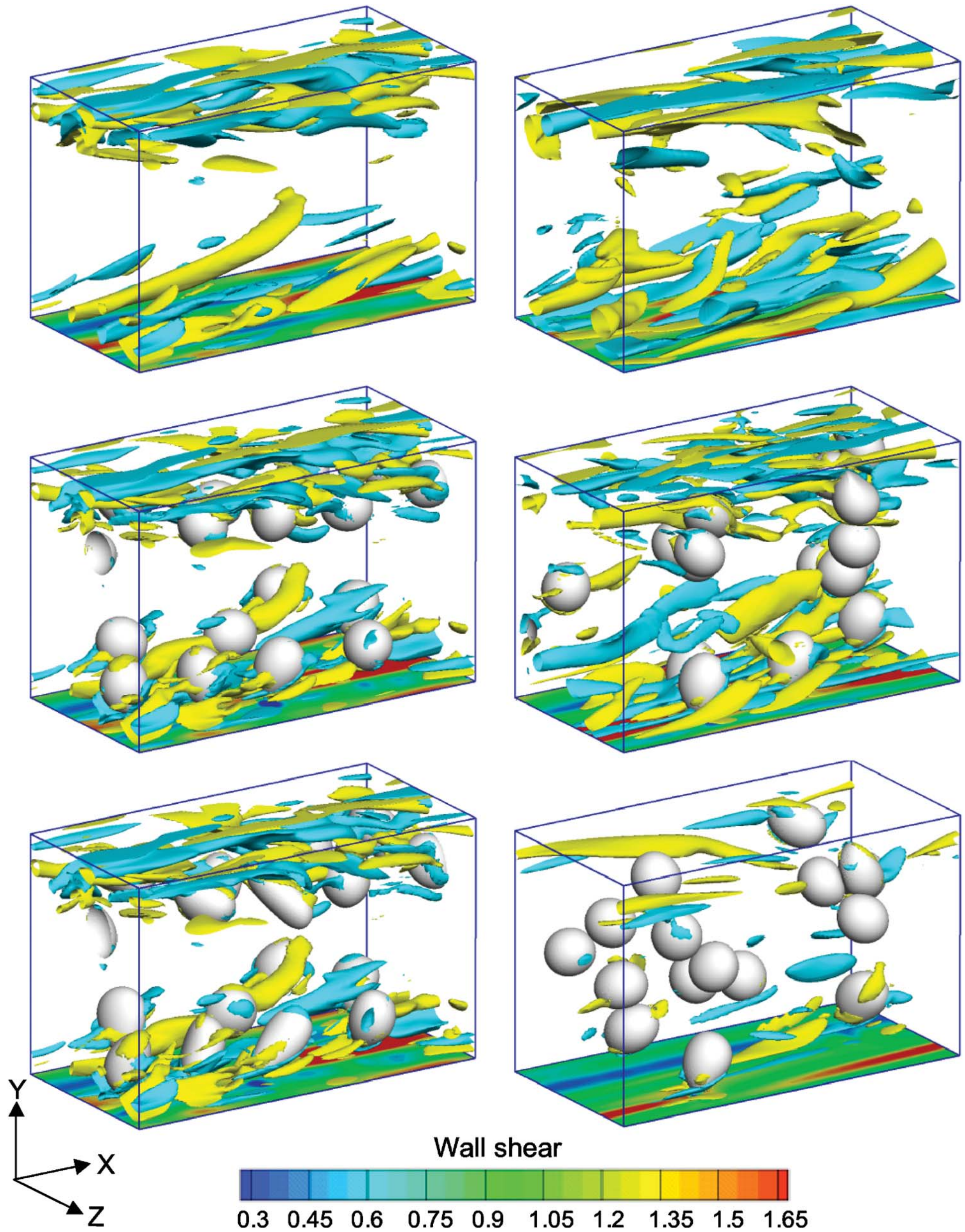

FIG. 1. (Color). The bubbles and isocontours of the streamwise vorticity for the flows without bubbles (top row) for We=0.203 (middle row) and We=0.405 (bottom row). The left column shows the flow at an early time =24.3 and the right column is at time =267.3, after the bubbles have had time to modify the flow. The isosurfaces represent the streamwise vorticities of 0.181 (yellow) and −0.181 (blue), nondimensionalized by $1/t^+$. The shear on the bottom wall is also shown (color scale is nondimensionalized by the average shear in the absence of bubbles). Red denotes high shear and it is clear that at a late time the shear for the We=0.405 case is smaller than when there are no bubbles.

the top wall has increased again slightly near the end of the simulation. The drag for the least deformable bubbles (We =0.203), on the other hand, increases rapidly after the initial adjustment phase and while it decreases again later, particularly on the top wall, it is always higher than for the flow without bubbles. The intermediate case (We=0.270) first shows drag increase, then falls below the no-bubble case at time 180 or so, but not to the level seen for the more deformable bubbles. Near the end of the simulation the drag on the top wall has increased again for this case. We note, as a reference, that if the bubbles completely relaminarized the flow, the drag would be reduced to about one-third of the total average drag in the absence of bubbles. To assess the changes that the addition of bubbles have on the turbulence, we have computed the autocorrelation function for both the flows with and without bubbles and confirmed that it is not changed significantly when the bubbles are added and that it shows a similar decay as reported in Ref. 16.

The increase in the wall shear in turbulent flows over laminar flows is due to the transfer of high-momentum fluid to the wall by nonzero wall-normal velocity fluctuations. Thus, it is natural to look at the $\langle u'v' \rangle$ component of the Reynolds stress tensor and how the bubbles change it. Here, u' is the instantaneous velocity fluctuation in the streamwise direction and v' is the fluctuation in the wall-normal direction. The Reynolds stresses are largest in the buffer layer, starting at about 10 wall units from the wall and reaching out to 50–100 wall units. In Fig. 4, the average of $\langle u'v' \rangle$ over planes parallel to the walls is plotted as a function of the wall-normal coordinate, for the flows with and without bubbles at two times. To give the reader a better feel for the relative size of the bubbles, we have drawn a circle with a diameter equal to that of the undeformed bubble on the figure. At both times the Reynolds stresses in the buffer layer, for the most deformable bubbles, are significantly below the

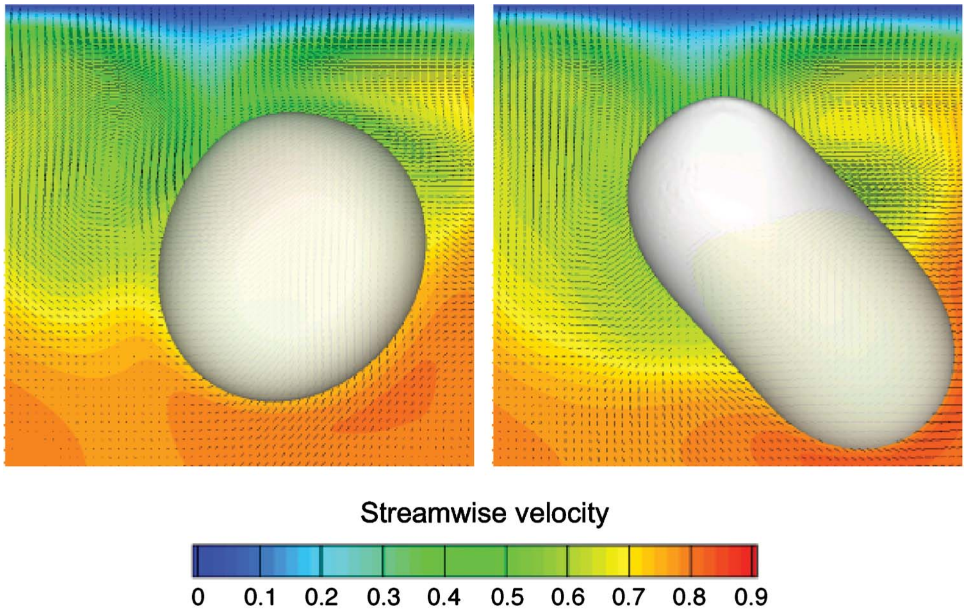

FIG. 2. (Color). Close-up of one bubble from the simulations shown in Fig. 1, at time=24.3. The flow in a plane perpendicular to the flow direction is shown by the vectors and the streamwise velocity is shown by the color contours. The bubble is near the top wall. Left frame: We=0.203; right frame: We=0.405.

no-bubble case. The curve for the other two cases is less conclusive: at the bottom wall the Reynolds stresses are very similar to the no-bubble results but the peak at the top wall has been reduced. We have plotted $\langle u'v' \rangle$ for a large number of intermediate times and generally find that it is lowest for the most deformable bubble and comparable to the no-bubble case for the less deformable bubbles. In Fig. 5 we plot the average of the absolute value of the Reynolds

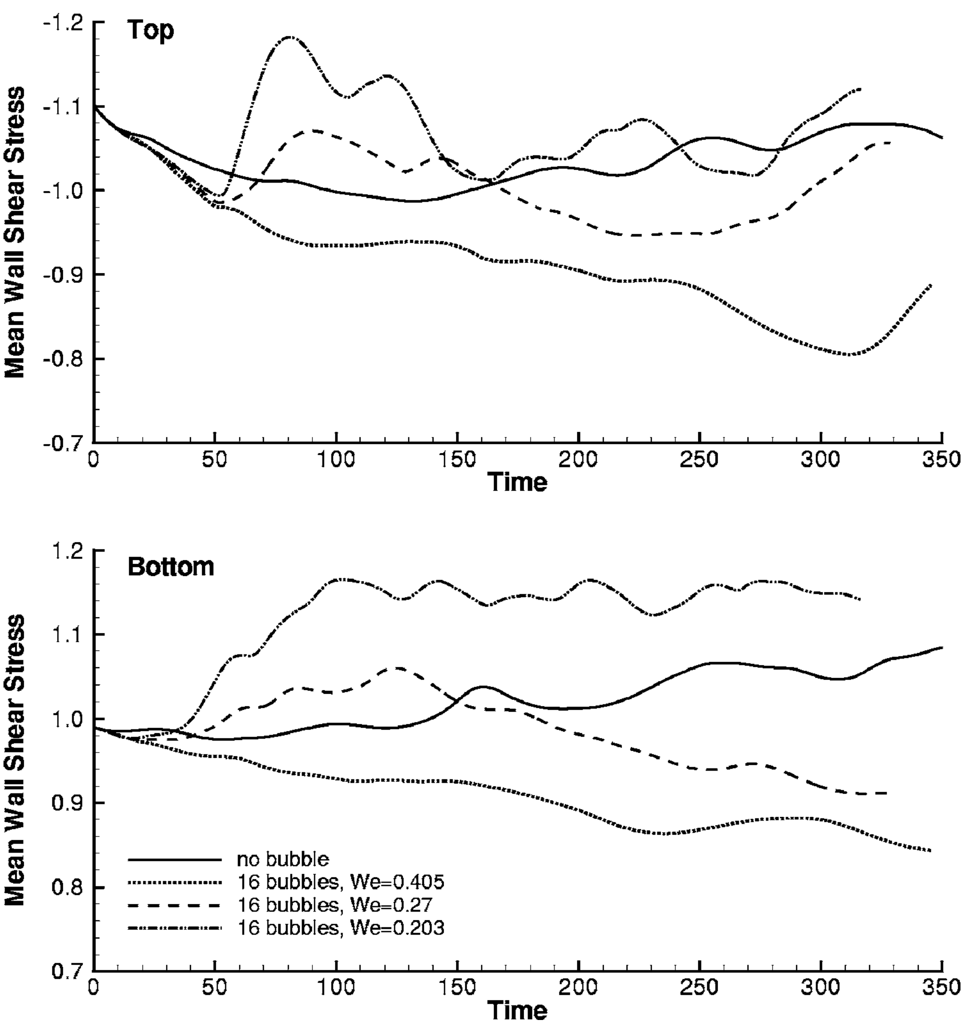

FIG. 3. The mean wall shear on the top and the bottom wall versus time for the flows with and without bubbles. For the no-bubbles case the average drag remains approximately constant but in the case with deformable bubbles there is a significant reduction in the wall drag. The shear stress is nondimensionalized by the average shear stress for the flow without bubbles.

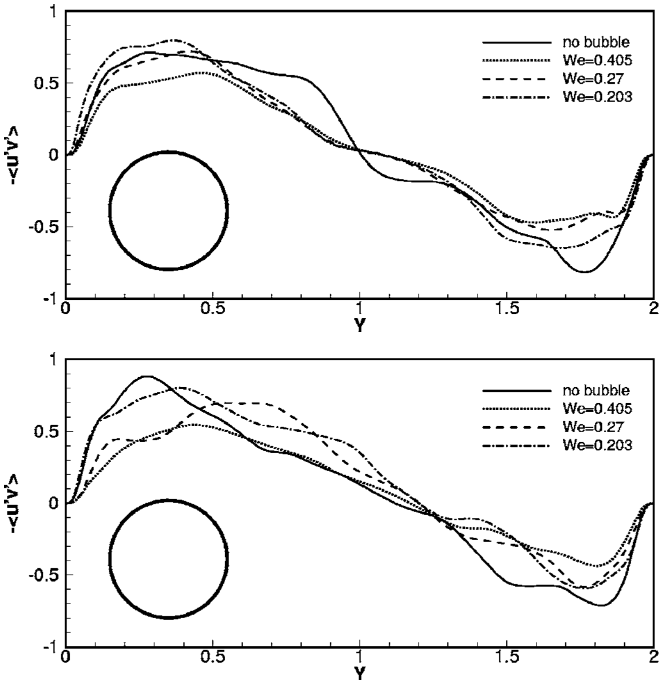

FIG. 4. The $\langle u'v'\rangle$ component of the Reynolds stresses versus the distance from the bottom wall, obtained by averaging over planes parallel to the wall, for all four simulations. The top frame is at time=97.2 and the bottom frame at time=243. The circle shows the size of an undeformed bubble. The Reynolds stresses are nondimensionalized by the friction velocity squared $(u^{+})^2$.

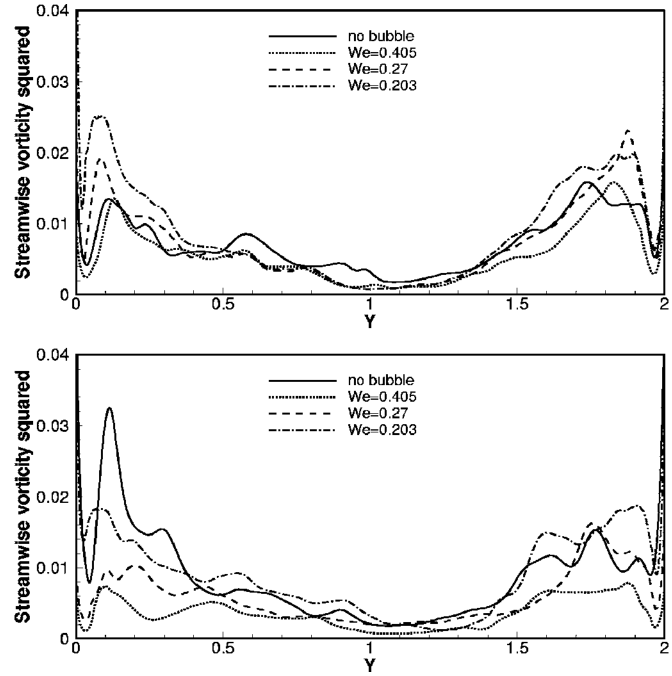

FIG. 6. The average streamwise vorticity, nondimensionalized by $(1/t^{+})^2$ at two times versus the wall-normal coordinate, obtained by averaging over planes parallel to the wall, for all four simulations. The top frame is at time=24.3 and the bottom frame at time=243.

stresses over the computational domain versus time for all four runs, with and without bubbles. The Reynolds stresses for the most deformable bubbles are always significantly lower than for the flow without bubbles, but for intermediate deformability the relation between the Reynolds stresses and the total drag is not very strong. The large initial drag increase due to the least deformable bubbles is, for example, not very visible in the graph.

While the Reynolds stresses change as the bubbles are added and drag reduction correlates with smaller $\langle u'v'\rangle$, the correlation is not as direct as one might perhaps wish. In any case, just plotting $\langle u'v'\rangle$ does not illuminate the physical mechanism for the change in the drag. As the suppression of the streamwise vorticity in Fig. 1 is the most striking difference between cases with drag reduction and without drag reduction, it is reasonable to look at the streamwise vorticity. In Fig. 6 we therefore plot the square of the streamwise vorticity, averaged over planes parallel to the walls, versus the wall-normal coordinate at two times. We plot the vorticity squared (the enstropy) since the streamwise vortices generally are of alternating signs. The vorticity is very high at the walls due to the wall-bounded vorticity necessary to bring the velocity induced by the streamwise vortices to zero. Then there is another maximum in the buffer layer due to the streamwise vortices and then there is decay toward the middle of the channel. At the early time, when only the most deformable bubbles result in drag reduction and the other bubbly cases show increased drag, there is considerable increase in the streamwise vorticity for the cases that show

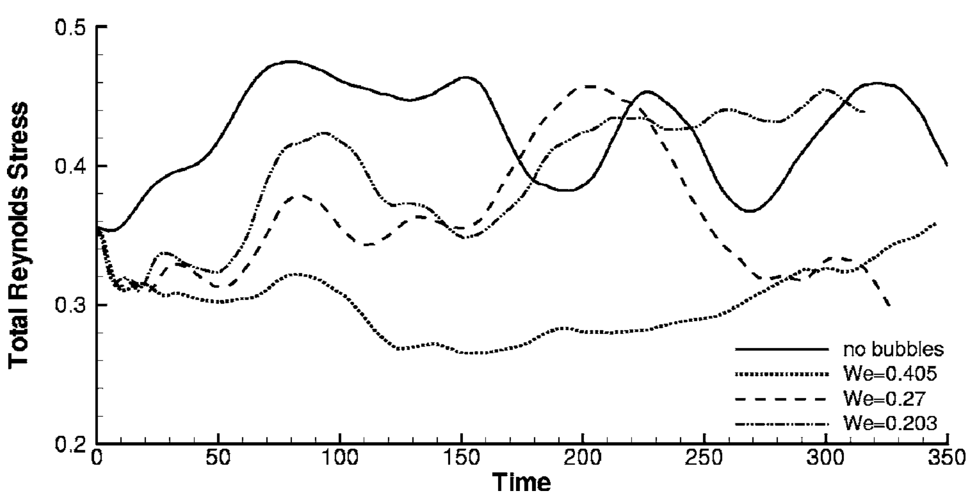

FIG. 5. The absolute value of the $\langle u'v'\rangle$ component of the Reynolds stresses, nondimensionalized by the friction velocity squared, $(u^{+})^2$, averaged over the computational domain, versus time for all four simulations.

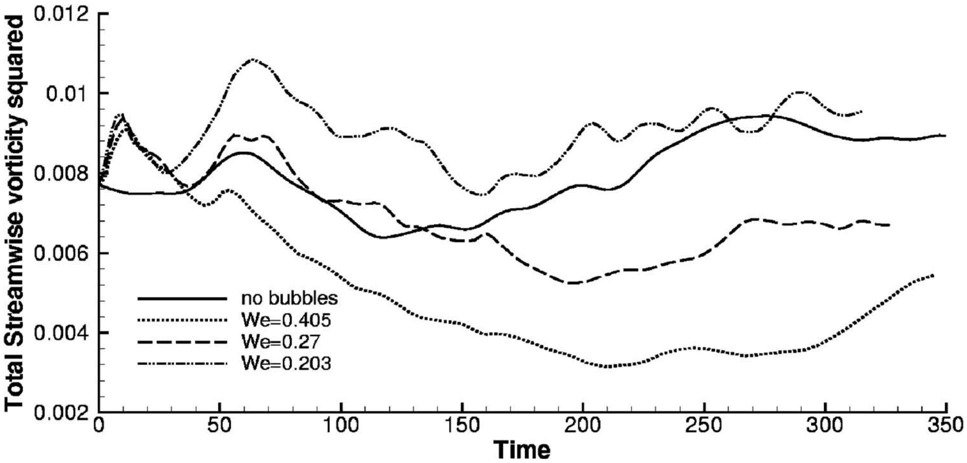

FIG. 7. The streamwise vorticity squared, nondimensionalized by $(1/t^{+})^2$, averaged over the computational domain, versus time for all four simulations.

drag increase and a slight reduction for the case with the most deformable bubbles. At the later time the reduction in the streamwise vorticity for the most deformable bubbles is significant. At any given time there are large fluctuations in the vorticity profile and while the total is obviously smaller in both cases, the pointwise values are not necessarily always smaller. In Fig. 7 we plot the integral of the streamwise vorticity squared, over the whole domain, versus time for the flows with and without bubbles. It is immediately clear that except for the initial transient, the evolution of the streamwise vorticity correlates well with the total drag. To reinforce the correlation between the streamwise vorticity and the total wall drag, the average drag versus the square of the streamwise vorticity, integrated over the computational domain for the simulation with the most deformable bubbles (We $=0.405$), at several evenly spaced times, is shown in Fig. 8.

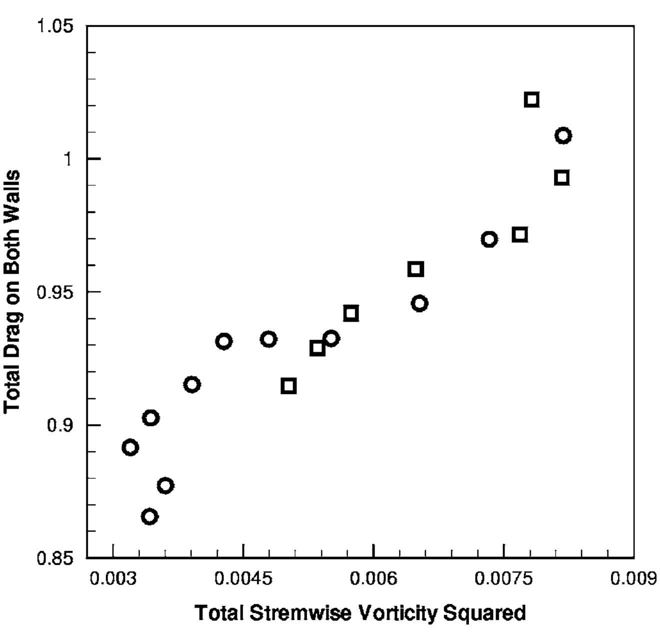

FIG. 8. The total drag on both walls (nondimensionalized by the average drag for the flow without bubbles) versus the total streamwise vorticity squared (enstropy), nondimensionalized by $(1/t^{+})^2$, computed at several times for the We$=0.405$ run. The circles are results from the 16-bubble simulation shown in Fig. 1. The squares are from another simulation with only four bubbles. As the enstropy is reduced, the drag decreases.

We have also included a few data points from another run with only four bubbles. Although the data have some scatter, it is clear that there is a direct relation between the decrease of the spanwise enstropy and the decrease in the wall drag. Another view of the reduction of the streamwise vorticity is shown in Fig. 9, where we plot the square of the wall-bounded streamwise vorticity, integrated over the top and bottom walls, versus time. This is the vorticity generated at the wall to satisfy the no-slip boundary conditions in the spanwise direction—not the streamwise direction—and as the total streamwise vorticity does, it correlates very well with the wall drag.

To examine the motion of the bubbles, we plot the wall-normal coordinate of the bubbles versus time in Fig. 10. The results for the We$=0.405$ bubbles are shown in the top frame and for the We$=0.203$ bubbles in the bottom frame. While some of the bubbles quickly move into the interior of the channel, others slide along the walls. In general the departure of some of the bubbles from the walls does not seem to strongly affect the drag, and by the end of the simulation of the most deformable bubbles, there is only one bubble left near the bottom wall, but the drag is still being reduced. While the bubbles gradually leave the wall, in some cases bubbles are carried to the wall again. Indeed, the close encounter of bubbles with the wall seems to be the main reason for the drag increase for the less deformable bubbles. A careful study of the bottom frame of the figure shows that several We$=0.203$ bubbles hit the top wall at around time 60 and again around time 120 when the drag increases sharply. Similarly, the drag increase on the bottom wall coincides with the presence of several bubbles close to the wall, although neither the change in bubble trajectory nor the increase in the drag is as dramatic as at the top wall. The drag increase at the top wall for the We$=0.203$ bubbles near the end of the simulation (around time 300) also coincides with the presence of bubbles close to the wall. The drag increase on the top wall for the most deformable bubbles near the end of the run, on the other hand, appears to be due to all the bubbles leaving the wall. Generally we find that the less deformable bubbles come closer to the wall than the most deformable ones. The minimum distance, for example, between the bottom wall and a bubble center is $1.321r_0$ (at

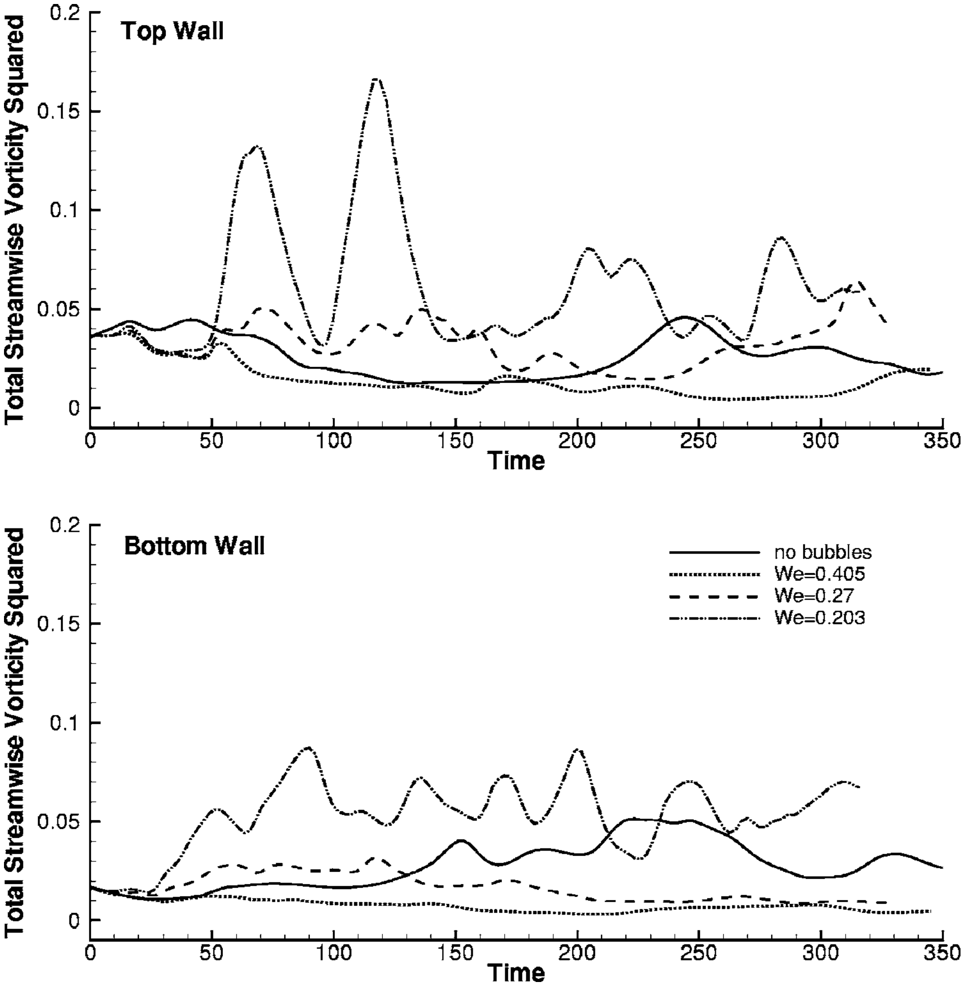

FIG. 9. The wall-bounded streamwise vorticity squared, nondimensionalized by $(1/t^+)^2$, integrated over the top and bottom walls, versus time.

around time 140) for We=0.405 and $1.068r_0$ (at time 235) for We=0.203. Here, r_0 is the radius of the nondeformed bubble. For the top wall the corresponding numbers are $1.103r_0$ (around time 170) for We=0.405 and $0.939r_0$ (at time 109) for We=0.203. Since the last distance is less than r_0, the bubble closest to the wall is obviously no longer spherical.

To quantify the bubble deformation we follow Bunner and Tryggvason[24] and compute the square root of the ratio of the largest and the smallest eigenvalue of the second moment of inertia tensor $\chi=(I_{\max}/I_{\min})^{1/2}$, where

$$I_{ij}=\frac{1}{\mathrm{vol}_b}\int_{\mathrm{vol}_b}(x_i-x_{io})(x_j-x_{jo})dV. \tag{3}$$

Here vol_b is the volume of the bubble and x_{io} and x_{jo} are the coordinates of the bubbles in the i- and j-coordinate directions. As in Ref. 24, the volume integrals are computed as surface integrals, using the divergence theorem. For modestly deformed ellipsoids, χ is approximately equal to the ratio of the smallest to the longest axis. For more complex bubble shapes, χ is a more general definition of the bubble deformation than the ratios of the longest and the shortest axis and eliminates any uncertainty in identifying those axis. In Fig. 11, we plot the deformation as defined by Eq. (3) versus the distance of the bubble centroid from the nearest wall for the most and least deformable bubbles. The plot was generated by sampling five evenly spaced times for each run, starting at time 50. Sampling the data more frequently results in the same trends, but a more crowded plot. The plot shows clearly that on the average the We=0.203 bubbles are significantly less deformed for a given distance from the wall. There are, however, more We=0.203 bubbles located in the high shear region next to the wall where their deformations increase, frequently matching the deformation of the We =0.405 bubbles further away from the wall. Far away from the walls, where the fluid shear is small, the deformations of all the bubbles are small and the We=0.203 bubbles, in particular, are essentially spherical.

The velocity of the bubbles, versus their location in the wall-normal direction is shown in Fig. 12 at time 97.2 (left column) and at time 267.3 (right column) for the most and least deformable bubbles, We=0.405 (top row) and We =0.203 (bottom row), respectively. The average fluid velocity, calculated by averaging over planes parallel to the walls, at each time is also shown. At the early times most of the bubbles are still close to the walls but at the later times the bubbles are more uniformly spread over the interior of the channel. For the most deformable bubbles, the center of the bubble closest to the wall is at $1.37r_0$, so there is a significant space between the bubble surface and the wall. The less deformable bubbles are slightly closer at time 97.2, when the closest We=0.203 bubble is only $1.135r_0$ from the top wall.

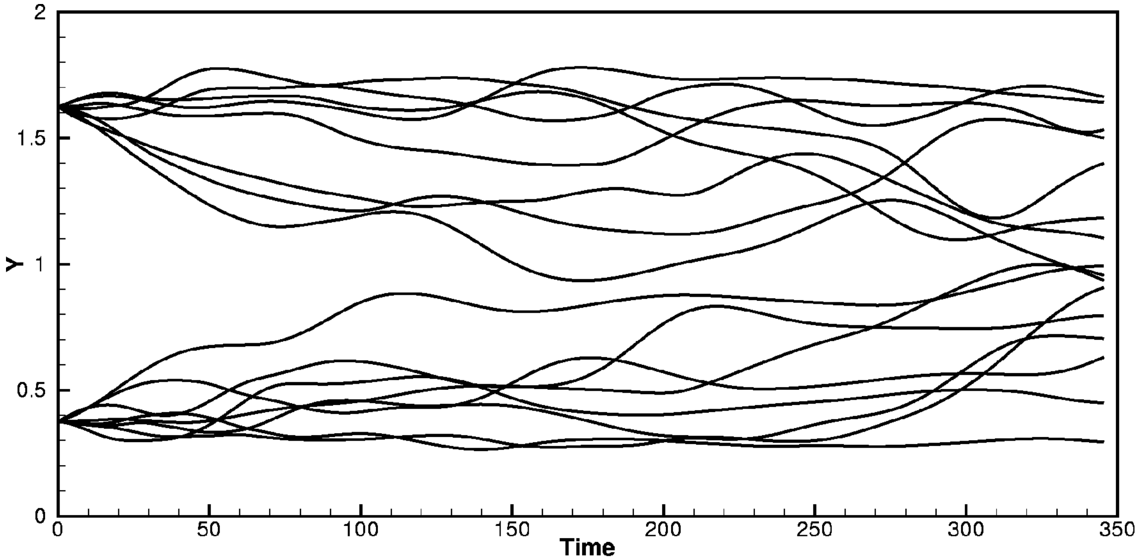

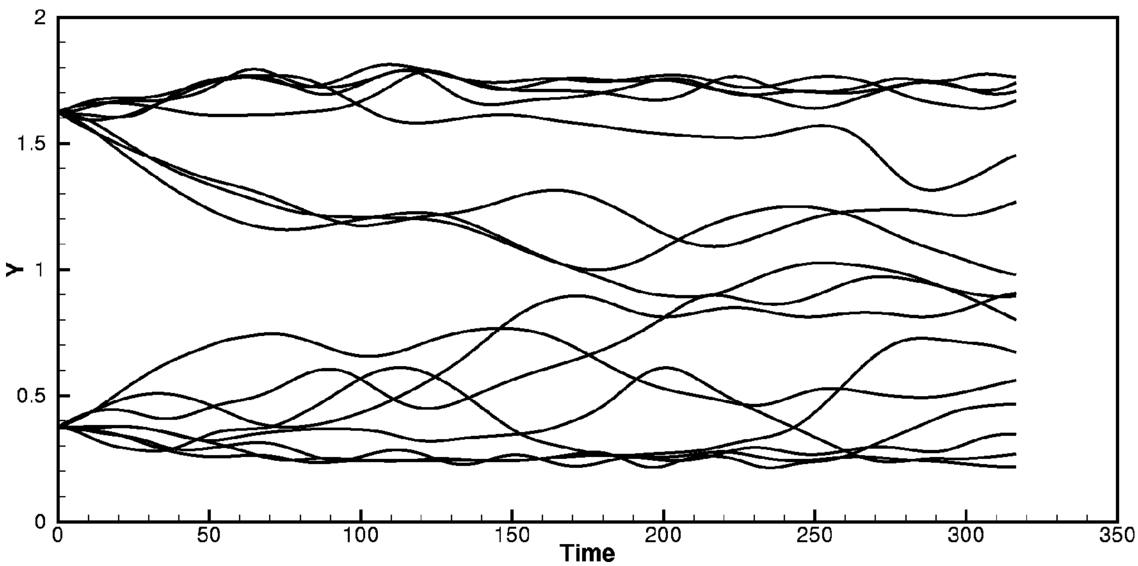

FIG. 10. The wall-normal coordinate of the bubbles versus time for We=0.405 (top frame lines) and We=0.203 (bottom frame).

As noted above, this coincides with a particularly large drag on the top wall. For the most part the bubbles move with essentially the average fluid velocity and there is relatively little slip between the bubbles and the average fluid motion. What slip there is, however, is largest for the least defomable bubbles that are near the walls. We have computed the relatively velocity between the bubbles and the average fluid velocity for a few times for the We=0.203 and the We =0.405 runs and plot the results in Fig. 13. The figure confirms that on the average the bubble velocity is always smaller than the fluid velocity and, on the average, the slip velocity of the least deformable bubbles is higher than for the most deformable ones, particularly near the end of the simulations. The least deformable bubbles are slowed down by partially penetrating into the slow moving fluid near the wall. The bubble average velocity is therefore smaller than the average fluid velocity and the bubbles hinder the fluid motion.

We have conducted a few other simulations using fewer bubbles and different size bubbles. We find that even four bubbles in the minimum turbulent channel can lead to comparable drag reduction, as long as the bubbles can deform. This is consistent with Fig. 1 where several bubbles have migrated to the interior of the channel and only a few bubbles are located near the walls, where they can influence the streamwise vortices. Relatively nondeformable bubbles, on the other hand, usually do not lead to drag reduction and can frequently increase the drag, particularly when they are close to the walls. Smaller bubbles also seem to have smaller effect than the bubbles shown in Figs. 1–3, although we have not done an exhaustive study of the effect of the bubble size.

The streamwise vortical structures found in turbulent boundary layers are generally separated by of the order of 100 wall units and the diameter of the vortex cores is considerably smaller. Bubbles smaller than the core diameter are likely to be drawn into the vortex core, but bubbles of the size considered here, where the Stokes number is much larger than unity, are unlikely to be strongly affected by the

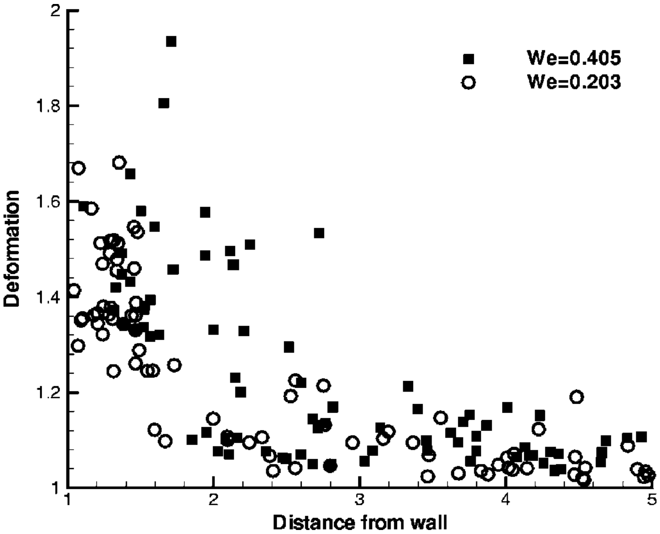

FIG. 11. The deformation of the bubbles [defined by Eq. (3)] versus the distance of the bubble centroid (nondimensionalized by the radius of the initially spherical bubbles) from the nearest wall, for the most (We =0.405) and least (We=0.203) deformable bubbles, at five evenly spaced times.

vortex cores. Thus, while the bubbles are certainly moved by the turbulent flow, their motion is not controlled by the smallest turbulence scales.

We have continued the simulation of the We=0.405 bubbles using a coarser grid and find that eventually the bubbles drift away from the wall and the drag reduction disappears. While the results on the coarser grid are not as accurate, they agree reasonably well with the results on the finer grid for the early time and we thus believe that the coarse grid long-time results are indicative of what would happen if the simulation presented here were continued. To reduce the possibility that the results depend sensitively on the particular flow configuration at time zero, we have also inserted the bubbles at a later time (but using the lower grid resolution) and found drag reduction. While the "minimum turbulent channel" is a rather special turbulent flow in that large asymmetries generally exist between the averaged flow properties across the channel, we see drag reduction at both walls, thus increasing the probability that the observed effects are generic. Furthermore, since the effect of the bubbles is modification of turbulence in the buffer layer, it seems reasonable to assume that enlarging the core region of the channel would not have a significant effect.

In our simulations the drag reduction eventually disappears as the bubbles disperse from the wall, and in a boundary layer, where bubbles are injected at a fixed location, the effect of the bubbles diminishes as one moves downstream from the injection point. While the persistence of drag reduction is obviously of immense technical significance, the considerations involved in persistence are likely to be different from those addressed here (involving primarily the dispersion of the bubbles by the turbulence) and if a mechanism could be found to keep the bubbles near the wall (such as injecting under a downward facing plate) there is no reason that the mechanism suggested here could not lead to drag reduction that would last for a long time.

We believe that the results presented in this section allow us to sketch a reasonably coherent, although perhaps preliminary, cartoon of how bubbles that are relatively large compared to the size of the buffer layer modify the turbulence near the wall in such a way that drag is reduced: Bubbles moving parallel to the wall, with a distance of about one bubble radius between the bubble surface and the wall, move

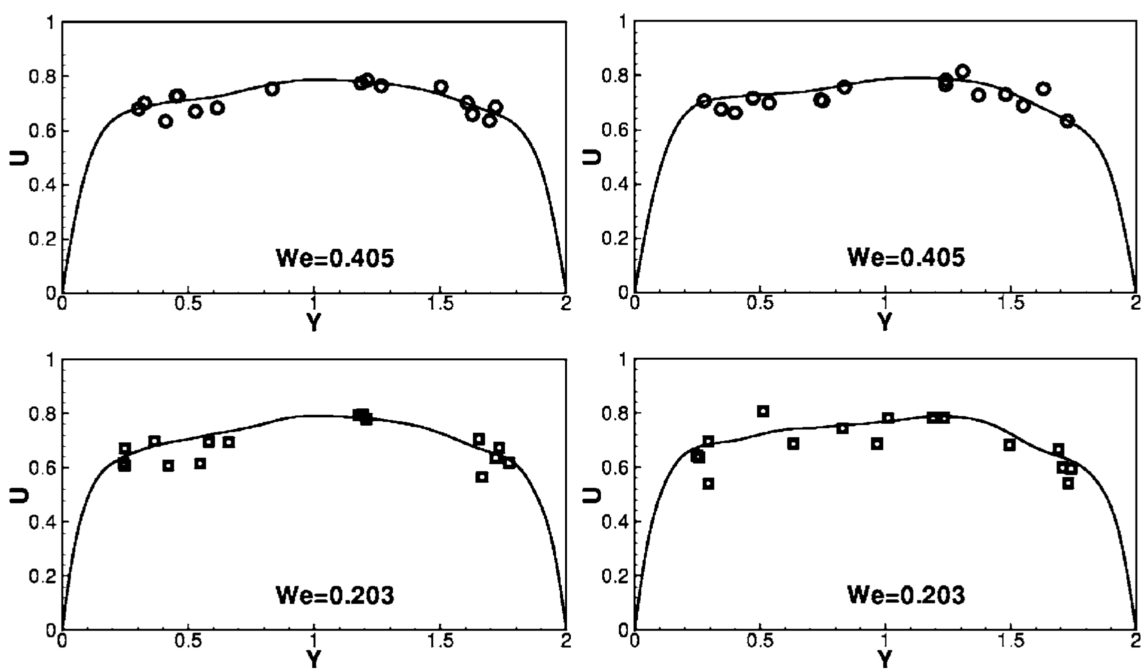

FIG. 12. The bubble velocity and the average fluid velocity, nondimensionalzed by U (the maximum laminar velocity at the same through flow), at two times for the most deformable bubbles (top row) and the nearly spherical bubbles (bottom row). The left frames are at time=97.2 and the right frames are at time=267.3.

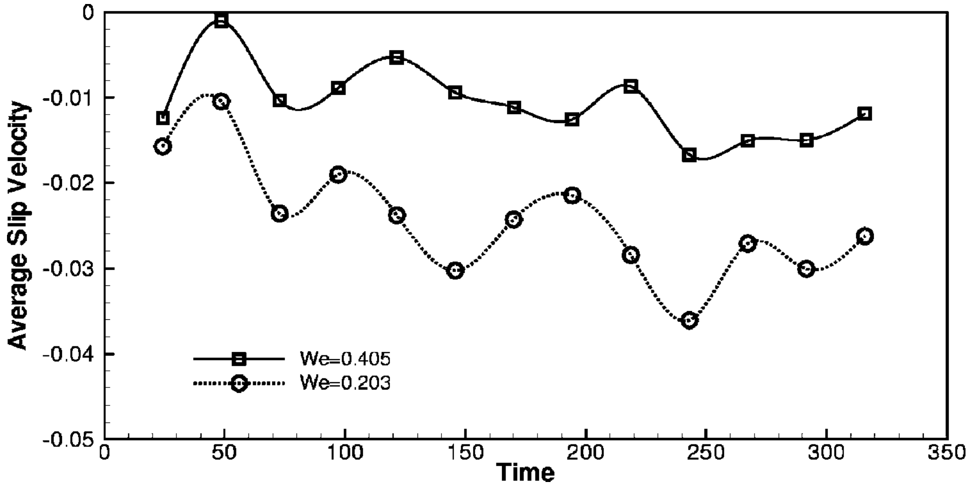

FIG. 13. The average slip velocity, nondimensionalized by U (the maximum laminar velocity at the same through flow), versus time for We =0.405 (solid lines) and We=0.203 (dashed lines). The slip is calculated at the times marked by a circle and a smooth curve has been fitted through the data points.

over streamwise vortices with a velocity that is higher than the advection velocity of the vortices. The passing of the bubbles forces the streamwise vortices closer the wall, squeezing them toward the wall and causing mutual cancellation between the streamwise vortices and the wall-bounded vorticity of the opposite sign. This results in a reduction of the streamwise vorticity and therefore a reduction of the $\langle u'v' \rangle$ component of the Reynolds stress tensor. To be effective, the bubbles must be at the right distance from the wall, and the more deformable bubbles appear to be able to slide along the wall at the right distance. The less deformable bubbles, on the other hand, are slowed down by reaching into the viscous sublayer and therefore act as obstacles to the faster moving liquid in the buffer layer. This increases drag significantly and the absence of a long smooth "glide" over the wall does not allow them to induce vorticity cancellation.

CONCLUSIONS

The main conclusion of the present work is that bubbles of a size comparable to the buffer layer in a low Reynolds number turbulent flow can generate significant drag reduction. The results also show that bubble deformability plays a major role in determining exactly how the bubbles affect the turbulence. While there is considerable evidence[4,12] that very small bubbles (diameter of a few wall units) reduce drag, bubbles injected into turbulent flow are frequently much larger.[15] Yet, drag reduction is observed for these situations. The mechanism proposed here explains how bubbles of a size comparable to the buffer layer lead to drag reduction. The net result—the suppression of the turbulence—is, however, also found in other drag reduction methods including polymer injection,[10] spanwise oscillations of the wall,[9] and injections of an order of magnitude smaller bubbles.[12]

Although these simulations are motivated in part by the experiments reported in Ref. 15, the conditions are not identical. The Reynolds number is obviously much lower here and we have examined a channel flow instead of a boundary layer. However, the flow rate is kept constant here and since the effect of the bubbles is confined to the region very near the wall, the difference in the flow configuration away from the wall should not have a major effect. The same argument applies to the Reynolds number. The nondimensional parameters describing the bubbles are, on the other hand, relatively close. For a tunnel velocity of 12.76 m/s, the friction velocity reported in the experiment was about 0.4 m/s and the mean bubble diameter was 300 μm. Thus, $d^+=120$ and We $=0.686$. While both are higher than the corresponding parameters used in this study, in part because the small size of the channel limits the size of the bubbles that can be considered to be minimally affected by the other wall, the values are nevertheless not too far off. We have also estimated the Stokes number of the bubbles and the near-wall void fraction in our simulations and in the experiment and find that they are of the same order of magnitude. Thus we expect that the conclusions reached here will apply to the situation studied in Ref. 15. We note that van den Berg *et al.*[25] have recently also concluded, based on experimental data, that deformability plays a major role in drag reduction by relatively large bubbles.

Although the study presented here provides an explanation for how bubbles can reduce skin friction drag in turbulent flows, there are obviously many aspects that remain to be addressed. The most obvious questions are what happens in a larger channel and how the drag reduction depends on the bubble size and the flow Reynolds number. While we do not have complete results for larger channels, we have done a few preliminary studies using a lower resolution that suggest that the drag reduction seen in the minimum channel also takes place in larger channels. These preliminary results do, however, also indicate that the modest changes in the turbulent characteristics, such as the spacing of the streamwise vortices, changes the effect that a bubble of a given size has on the flow. We have also done a few preliminary simulations to look at the effect of bubble size and generally find that making the bubbles smaller with constant surface tension (so the bubbles become less deformable) eliminates drag reduction, but reducing surface tension such that the Weber number is constant can preserve drag reduction, at least within the narrow range of parameters that we have examined. We note that in a realistic situation where air is injected through a hole in the wall and fluid shear tears off bubbles, most of the air is likely to be contained in bubbles whose size falls within a narrow range. The bubbles have to have reached a certain size for the shear to overcome surface tension and pull the bubbles off the wall, and in high shear large bubbles will break into smaller ones. There are, of course, complications. Small bubbles can be formed as a by-product when a large bubble is torn off the wall (when thin air filament breakup into small bubbles) and bubbles can coalesce. However, the photographs in Ref. 15 seem to support the above argument for a relatively narrow size distribution, at least to the lowest order.

ACKNOWLEDGMENTS

This work was supported by the Defense Advanced Research Projects Agency, Advanced Technology Office, under the Friction Drag Reduction Program, as a subaward SO4-16 to Contract No. HR0011-04-C-0011 to Pennsylvania State University. Some of the computations were done at the WPI Center for Parallel Computing and using computer resources allocated by NPACI. We are grateful to J. Xu, M. R. Maxey, and G. E. Karniadakis at Brown University for providing the initial turbulent data.

[1]M. E. McCormick and R. Bhattacharyya, "Drag reduction of a submersible hull by electrolysis," Nav. Eng. J. **85**, 11 (1973).
[2]N. K. Madavan, S. Deutsch, and C. L. Merkle, "Measurements of local skin friction in a microbubble-modified turbulent boundary layer," J. Fluid Mech. **156**, 237 (1985).
[3]N. K. Madavan, S. Deutsch, and C. L. Merkle, "Reduction of turbulent skin friction by microbubbles," Phys. Fluids **27**, 356 (1984).
[4]C. L. Merkle and S. Deutsch, "Drag reduction in liquid boundary layers by gas injection," in *Viscous Drag Reduction in Boundary Layers*, edited by D. M. Bushnell and J. N. Hefner, Progress in Astronautics and Aeronautics, vol. 123 (AIAA, Reston, VA, 1990), pp. 351–412.
[5]Y. Kodama, A. Kakugawa, T. Takahashi, S. Nagaya, and K. Sugiyama, "Microbubbles: Drag reduction and applicability to ships," in *Twenty-Fourth Symposium on Naval Hydrodynamics* (National Academies Press, Washington, DC, 2003), available at http://books.nap.edu/catalog/10834.html.
[6]H. H. Legner, "A simple model for gas bubble drag reduction," Phys. Fluids **27**, 2788 (1984).
[7]M. Lance and J. Bataille, "Turbulence in the liquid phase of a uniform bubbly air-water flow," J. Fluid Mech. **222**, 95 (1991).
[8]G. Sridhar and J. Katz, "Effect of entrained bubbles on the structure of vortex rings," J. Fluid Mech. **397**, 171 (1999).
[9]Y. Du and G. Em. Karniadakis, "Suppressing wall turbulence by means of a transverse traveling wave," Science **288**, 1230 (2000).
[10]T. Min, J. Y. Yul, H. Choi, and D. D. Josephs, "Drag reduction by polymer additives in a turbulent channel flow," J. Fluid Mech. **486**, 213 (2003).
[11]J. Xu, M. R. Maxey, and G. Em. Karniadakis, "Numerical simulation of turbulent drag reduction using micro-bubbles," J. Fluid Mech. **468**, 271 (2000).
[12]A. Ferrante and S. E. Elghobashi, "On the physical mechanisms of drag reduction in a spatially developing turbulent boundary layer laden with microbubbles," J. Fluid Mech. **503**, 345 (2004).
[13]A. Kanai and H. Miyata, "Direct numerical simulations of wall turbulent flows with microbubbles," Int. J. Numer. Methods Fluids **35**, 593 (2001).
[14]T. Kawamura and Y. Kodama, "Numerical simulation method to resolve interactions between bubbles and turbulence," Int. J. Heat Fluid Flow **23**, 627 (2002).
[15]W. C. Sanders, D. R. Dowling, M. Perlin, and S. L. Ceccio, "Bubble friction drag reduction in a high reynolds number flat plate turbulent boundary layer," J. Fluid Mech. (to be published).
[16]J. Jimenez and P. Moin, "The minimal flow unit in near-wall turbulence," J. Fluid Mech. **225**, 213 (1991).
[17]S. O. Unverdi and G. Tryggvason, "A front-tracking method for viscous, incompressible, multi-fluid flows," J. Comput. Phys. **100**, 25 (1992).
[18]G. Tryggvason, B. Bunner, A. Esmaeeli, D. Juric, N. Al-Rawahi, W. Tauber, J. Han, S. Nas, and Y.-J. Jan, "A front tracking method for the computations of multiphase flow," J. Comput. Phys. **169**, 708 (2001).
[19]B. Bunner and G. Tryggvason, "Dynamics of homogeneous bubbly flows: Part 1. Rise velocity and microstructure of the bubbles," J. Fluid Mech. **466**, 17 (2002).
[20]B. P. Leonard, "A stable and accurate convective modelling procedure based on quadratic upstream interpolation," Comput. Methods Appl. Mech. Eng. **19**, 59 (1979).
[21]M. Rudman, "A volume-tracking method for incompressible multifluid flows with large density variations," Int. J. Numer. Methods Fluids **28**, 357 (1998).
[22]The initial turbulent data were provided by J. Xu, M. R. Maxey, and G. Em Karniadakis at Brown University.
[23]P. Orlandi, *Fluid Flow Phenomena. A Numerical Toolkit* (Kluwer Academic, Dordrecht, 2000).
[24]B. Bunner and G. Tryggvason, "Effect of bubble deformation on the stability and properties of bubbly flows," J. Fluid Mech. **495**, 77 (2003).
[25]T. H. van den Berg, S. Luther, D. P. Lathrop, and D. Lohse, "Drag reduction in bubbly Taylor-Couette turbulence," Phys. Rev. Lett. **94**, 044501 (2005).